

Skin-Screen: A Computational Fabrication Framework for Color Tattoos

MICHAL PIOVARČI, ISTA, Austria

ALEXANDRE CHAPIRO, Independent, Brazil

BERND BICKEL, ISTA, Austria

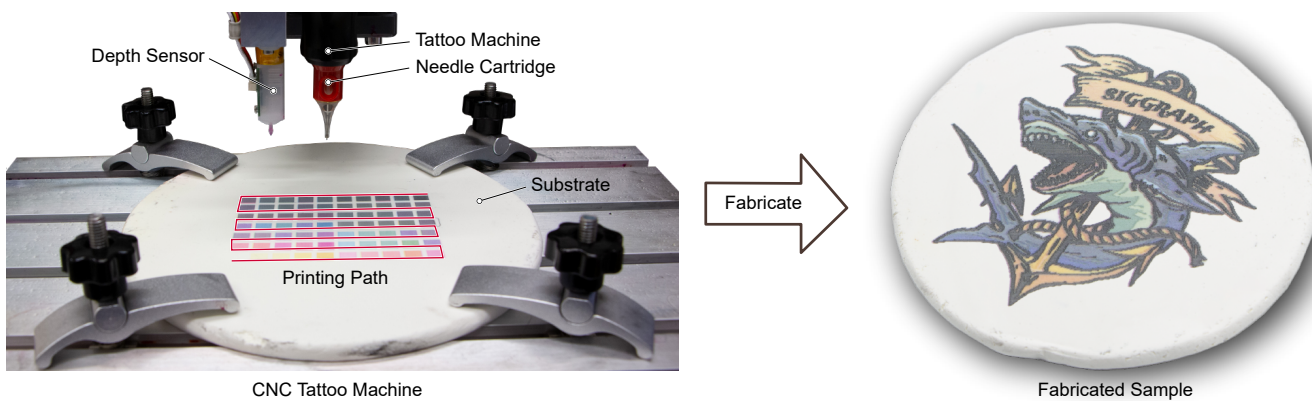


Fig. 1. We developed a numerically controlled tattooing machine to enable the systematic study of tattooing as a fabrication process.

Tattoos are a highly popular medium, with both artistic and medical applications. Although the mechanical process of tattoo application has evolved historically, the results are reliant on the artisanal skill of the artist. This can be especially challenging for some skin tones, or in cases where artists lack experience. We provide the first systematic overview of tattooing as a computational fabrication technique. We built an automated tattooing rig and a recipe for the creation of silicone sheets mimicking realistic skin tones, which allowed us to create an accurate model predicting tattoo appearance. This enables several exciting applications including tattoo previewing, color retargeting, novel ink spectra optimization, color-accurate prosthetics, and more.

CCS Concepts: • Computing methodologies → Reflectance modeling;
• Hardware → Modeling and parameter extraction.

Additional Key Words and Phrases: appearance, modeling, reproduction, tattoo, skin color, gamut mapping, ink-optimization, prosthetic

ACM Reference Format:

Michal Piovarči, Alexandre Chapiro, and Bernd Bickel. 2023. Skin-Screen: A Computational Fabrication Framework for Color Tattoos. *ACM Trans. Graph.* 42, 4, Article 1 (August 2023), 13 pages. <https://doi.org/10.1145/3592432>

1 INTRODUCTION

Tattooing is a popular technique, wherein a pattern is permanently inscribed on the subject's skin through the subcutaneous deposition

Authors' addresses: Michal Piovarči, michael.piovarci@ist.ac.at, ISTA, Austria; Alexandre Chapiro, alex@chapiro.net, Independent, Brazil; Bernd Bickel, bernd.bickel@ist.ac.at, ISTA, Austria.

Permission to make digital or hard copies of part or all of this work for personal or classroom use is granted without fee provided that copies are not made or distributed for profit or commercial advantage and that copies bear this notice and the full citation on the first page. Copyrights for third-party components of this work must be honored. For all other uses, contact the owner/author(s).

© 2023 Copyright held by the owner/author(s).

0730-0301/2023/8-ART1

<https://doi.org/10.1145/3592432>

of ink via a needle. Researchers have discovered tattoos as old as 5,400 years [McGill University 2017], and the art form continues to be highly popular around the world today. For instance, 48% of Italians, 47% of Americans, and 46% of Swedes report having tattoos. 21,000 tattoo parlors are reportedly operating in the USA today, where the tattooing industry generates an estimated \$1.6 billion in revenue yearly [Zuckerman 2020]. In addition to purely artistic designs, tattooing is also used for cosmetic or medical purposes.

While the mechanical means of applying tattoos have seen significant historical evolution, such as the introduction of the electronic tattoo gun in the late 19th century and subsequent improvements, the artistic process remains broadly similar to its historic roots. Tattoo artists plan and execute designs in an artisanal fashion, and the accuracy of the result depends largely on the skill and experience of the artist. As the medium of a tattoo is the subject's skin, the resulting color depends on both the pigments used by the artist and the subject's complexion. Notably, it is generally considered more difficult to reproduce colorful designs on darker skin tones. Due to the complex social issues surrounding skin color, a technical discussion on the feasibility of tattoos is often considered taboo [Withee 2018]. As artists may be reluctant to experiment with color due to the permanent nature of tattooing, this further compounds the difficulty of creating the knowledge base required for high-quality color tattoos for varying skin tones. One of the goals of this work is to enable a quantitative understanding of tattooing, allowing for inclusive techniques to be developed.

Further, we set out to provide a systematic overview of the tattooing process as a medium for computational fabrication. Beyond traditional tattoos, we explore needle ink deposition as a tool for full-color texture generation. We begin by constructing a highly controllable computational tattooing rig. By borrowing techniques

from the tattoo artist training repertoire, we generate representative silicon-based skin alternatives that are used to build a first-of-its-kind model predicting tattoo appearance. We demonstrate our model's utility to several novel applications, including tattoo previewing, tattoo color remapping for a target skin tone, novel tattoo ink spectrum generation, silicon prosthetic fabrication, and functional tattooing.

2 RELATED WORK

While no prior art on the treatment of tattooing within a computational framework exists, our work can be discussed in the historic and practical context of tattooing (Sec. 2.1), engineering treatments of color (Sec. 2.2 and Sec. 2.3), and appearance modeling for computational fabrication (Sec. 2.4).

2.1 Tattoos in the Arts and Medicine

As an artistic medium, tattoos have a long and fascinating history beginning over 5,400 years ago and continuing through a recent global rise to popularity and commercial relevance. From a sociological perspective, artistic tattooing has been extensively discussed in terms of history, appeal, and perceived social acceptability [Sanders and Vail 2008]. Although discussion on technical or social aspects of tattoos on subjects with varying skin tones is largely absent, many popular articles are dedicated to this subject online [Munce 2021]. Discussion often centers around commonly held beliefs about the feasibility of color tattoos on darker skin tones, but most often the topic is obscured by the lack of quantitative modeling and generally regarded as a sensitive subject [Withee 2018]. We hope techniques like the one presented in this work lead to a more inclusive environment, augmenting artists' practical experience with simulation and visualization tools.

The medical applications of tattoos, including both cosmetic and medicinal purposes, have been discussed by Vassileva and Hristakieva [2007]. Micropigmentation, or "permanent makeup" techniques, are commonly used as a camouflaging tool in the management of diseases like vitiligo or alopecia areata, or as a reconstructive tool for the masking of burn scars or nipple-areola reconstruction [Garg and Thami 2005]. These methods can benefit from a quantitative understanding of tattoo mechanics and the appearance simulation toolkit developed in our work. More recently, the use of tattooing techniques as a medium for the introduction of vaccines to the epidermal and dermal layers of skin has been discussed [Pokorna et al. 2008]. This type of technique may benefit from the use of a spatially- and depth-calibrated mechanical tattooing device like the one constructed in this work. Generally, allowing practitioners to preview and personalize solutions to patient needs while accounting for individual variability could lead to improved outcomes.

2.2 Models of Color

Color has long been a topic of scientific interest. For an overview of perceptual aspects and models of color vision, we recommend the classic book by Wyszecki and Stiles [1982].

A vast literature exists on accurate and predictable reproduction of color for paint mixtures on surfaces. We extend this by

seeking to faithfully reproduce desired colors in tattoos. The state-of-the-art in color prediction for printed media is the Neugebauer equations [Neugebauer 1937], enhanced with Yule-Nielsen corrections [Yule and Nielsen 1951]. To predict the visible color, the equations assume a linear mixture of ink spectra. While such an assumption is feasible for half-toned colors, that are mixed spatially, it does not hold for the tattoo process. As the needle enters the substrate depositing primary colors, they mix non-linearly.

Historically, a seminal model predicting the colors produced by physically mixing paints was proposed by Kubelka and Munk [1931]. This highly successful method relies on a spectral model of scattering and absorption and was introduced to the graphics community with the goal of realistic image synthesis [Haase and Meyer 1992]. It continues to be relevant for tasks like pigment mixing simulation for digital painting [Sochorová and Jamriška 2021].

The Kubelka–Munk model itself is a special case of the rendering equation. As shown by recent work in color 3D printing [Nindel et al. 2021], it is possible to use the full equation to improve color reproduction and minimize dot gain. However, in order to apply a full heterogeneous medium rendering, one needs to estimate the material composition of the medium. While voxelization is a good approximation for an inkjet printer, needle deposition is significantly more complex. The abrasion and absorption of the ink inside the substrate are unknown and would need to be modeled first. An alternative to modeling the ink deposition is a data-driven color predictor [Shi et al. 2018; Chen and Urban 2021]. Unfortunately, such predictors require hundreds of colors, making the methods impractical for experimental printing setups like ours, where a single measurable patch takes approximately 4 minutes to fabricate. Instead, we demonstrate that it is possible to achieve faithful color reproduction using a small set of measurements. We achieve this by adapting the Kubelka–Munk model to the context of tattoos.

In a computational context, color is often modeled through the use of color spaces, such as those maintained by the International Commission on Illumination (CIE). Several popular methods are used in this work, including the CIE La^*b^* and CIE XYZ color spaces and the ΔE_{00} color difference metric [Johnson and Fairchild 2003]. For an overview of mathematical approaches to color technology and colorimetry, we recommend Roy Berns' book [2019]. Colorimetric measurement has been employed in the study of skin tones by Weatherall and Coombs [1992]. However, as tattooing is not a trivial light-additive or subtracting medium, this information is not sufficient to accurately model the appearance of tattoo inks under the skin. Consequently, more sophisticated methods based on fitting parametric models of skin appearance to measured data were proposed [Donner et al. 2008; Lister et al. 2012; Finlayson et al. 2022]. Unfortunately, the models are closely tied to the measuring setups and can have variations of 2 orders of magnitude depending on the fitted parameters [Mignon et al. 2018]. As a consequence, applying analytical skin models to predict tattoo colors remains challenging.

2.3 Gamut Mapping

Notably, different media cannot necessarily represent the same set of colors, nor can any medium represent the set of all visible colors. The set of colors reproducible on a given output device is often referred

to as its color gamut. sRGB is an example of a popular standardized color gamut for digital displays [Anderson et al. 1996], which is used as a reference throughout this work. In our computational framework, the combination of tattoo ink and skin is treated as a color gamut and modeled using the associated techniques (Sec. 6).

As each reproduction technology can have unique color properties, often failing to reach a given standard, gamut mapping techniques are used to find the best match for the reproduction of an intended color in an output medium [Morovič 2008]. Traditionally, gamut mapping techniques differ in the treatment of so-called out-of-gamut colors. While simpler methods may opt to "clip" these values to the nearest boundary [Stone et al. 1988], this may cause undesirable artifacts. More advanced techniques eschew simple scaling and clipping and may enforce the preservation of the appearance of especially important colors, such as skin, grass, or sky tones [Kang et al. 2006]. An especially important point in any color gamut is its white point. This color coordinate represents neutral tones for a given system, and white point adaptation techniques [Luo and Hunt 1998] aim to mimic the equivalent effect in human vision, which serves to adjust the observer's vision to a given illuminant and helps maintain color constancy.

2.4 Appearance Reproduction in Fabrication

Computational fabrication has been an exciting topic of investigation in the computer graphics community. Recent methods investigate many aspects of appearance modeling for 3D-printed samples, such as translucency [Urban et al. 2019], gloss [Piovarci et al. 2020], and scattering [Papas et al. 2013].

Color has similarly been a topic of investigation in fabrication literature. Color fabrication using jet printers on surface isolayers via halftoning was employed by Brunton et al. [2015]. While this work presents relevant discussions on translucency and color reproduction, traditional printing is not possible for our application. In contrast to this technique, Babaei et al. [2017] use the Kubelka-Munk model to optimize the color appearance of layers of ink of different thickness inside a 3D-printed volume. This work has important parallels to our goals in tattoo modeling but also significant differences, as tattoos cannot be arbitrarily voxelized and the color of the substrate is fixed to the subjects' complexion. Recent work, [Elek et al. 2017; Sumin et al. 2019; Nindel et al. 2021] uses volume rendering to find the best parameters for color appearance reproduction for 3D prints. Our work employs a similar optimization toolkit to find the optimal ink parameters for tattoo color reproduction.

3 HARDWARE APPARATUS

To study the complex interaction between substrate and ink, we aim to build a data-driven model of tattoo appearance. Ink deposition in the skin is a complex process, with many practical factors such as depth, density, skin tone, and surface properties all playing a role. To conduct a quantitative investigation of the tattooing process, we developed a CNC tattooing platform, shown in Figure 1 left. The base of our platform is a 3-Axis Cartesian robot, which has a build area of 300×180 mm and a 10 micron step size. The payload of the robot is an electronic tattoo gun with a variable voltage from 4 V to 8 V. The voltage setting affects the frequency at which the

tattoo gun operates (between 35 and 90 Hz), as well as the depth of injection. The tattoo gun can be outfitted with cartridges that differ in the number of needles and orientation. We opted for a commercially-available model in which the needles are oriented in a circular configuration and have an approximate effective tattoo diameter of 209 microns.¹ We further enhanced the system using a depth sensor with an accuracy of ± 5 microns. The depth sensor is used to provide a dense height map of the substrate that serves as a zero surface. To generate a printing path for the machine, we follow a zig-zag space-filling curve.

During deposition, the ink-covered needle enters the substrate and, through a mechanism of absorption and abrasion, part of the ink remains entrapped within the material. The key properties governing the amount of deposited material are the scanning speed, spatial frequency of injections, and injection depth. These properties are inherently coupled. For example, altering the needle frequency is possible only by changing the voltage, which also affects the depth of the tattoo. Additional interactions between depth and scanning speed exist, for instance, high speeds coupled with high depth could damage the needle or substrate. To keep our investigation feasible, we decided to limit the free parameters. Specifically, we only control the liftoff of the tattoo needle by adjusting the Z-axis of the Cartesian robot. The remaining parameters, scanning speed (5 mm/s), zig-zag spacing (189 microns), and needle voltage (6 V), remain fixed. Overview of the tattoo process is depicted in Figure 2.

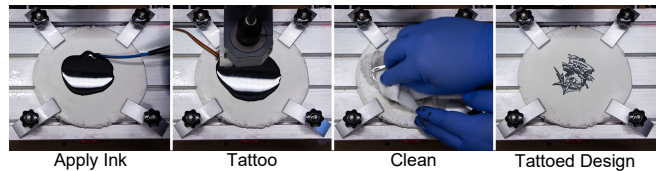


Fig. 2. To realize a physical tattoo, we repeat the same procedure for each applied ink. To tattoo a path, we first cover the substrate with a uniform layer of ink. Next, the design is tattooed. Afterward, we clean any remaining ink using WD-40 and de-grease the substrate with isopropanol.

As experiments with skin are undesirable, we conducted an exploration for alternatives via extensive conversations with professional tattooists. The most relevant medium for our work was found to be synthetic sheets, which are commercially used in replacing skin as training media for aspiring artists. However, commercial availability is limited and does not allow for arbitrary "skin" color selection desirable for our purpose. Consequently, we support the tattoo machine with a repeatable recipe for manufacturing tattoo substrates. The base of our tattoo sheets is silicone rubber. Since silicone is hydrophobic, it does not absorb tattoo inks, Figure 3 left. To increase the ink absorption, we mix the silicone in a 1:1 ratio by weight with corn starch, Figure 3 middle. Furthermore, we opted for the use of vinegar-cured silicone that is typically used in sanitary applications, Figure 3 right. The small amount of vinegar helps to better develop the colors and achieve higher color saturation.

¹Warrior 0.35mm 1203RL



Fig. 3. The effect of different substrate mixtures on color saturation.

To create a homogeneous mixture, we employ a bread-baking machine, Figure 4 top. The resulting mixture is rather stiff, similar in consistency to play dough, and does not allow for casting. To manufacture sheets of uniform thickness, we rely on a press, Figure 4 bottom left. We place a small quantity of the silicone in the middle and compress it for 24 hours after which the silicone is cured, Figure 4 bottom right. For inks, we rely on cyan, magenta, yellow, and black inkjet inks from Epson.² Although these are not perfect substitutes for tattoo inks and skin, we believe they provide a practical platform for tool development without loss of generality, which can be ameliorated via in-vivo testing in future work.



Fig. 4. The silicone and cornstarch are mixed together using the kneading program. We then place the final mixture in a press to create sheets with uniform height.

4 COLOR MODELING

Commercial color calibration relies on building color look-up tables from large datasets of colors. Typical color targets start at over 900 colors and can use even more to achieve a high-quality calibration [X-Rite 2005]. Unfortunately, the printing speed of our experimental setup is significantly slower than commercial color printers. Therefore, we seek a more sample-efficient method of building a predictive color model. More specifically, we rely on the

²Epson EcoTank 102 Standard

well-known Kubelka–Munk model. In this section, we will briefly introduce the model and describe how to apply it in the context of predicting tattoo colors. The overview of this process is depicted in Figure 5.

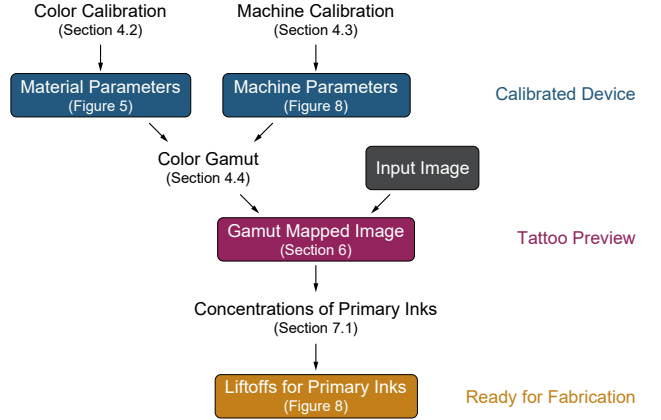


Fig. 5. To calibrate the device, we tattoo two patterns: one to estimate the material parameters for the substrate and the primary inks; and another to build a function mapping the machine parameters to ink concentrations. We can then sample the calibrated device (top row) to compute the color gamut. Using the color gamut, we can preview the tattoo designs (middle row). To physically realize the designs, we use the Kubelka–Munk model to estimate ink concentrations for gamut-mapped colors. Finally, we map the concentrations to tattoo machine liftoffs and generate a printing path for the machine (bottom row).

4.1 Color Predictive Model

Kubelka–Munk model assumes each ink p has intrinsic wavelength-dependent absorption $K_p(\lambda)$ and scattering $S_p(\lambda)$. The absorption and scattering of different inks mix linearly. Therefore, given a set of primary inks \mathcal{P} , an ink resulting from mixing the primaries in various proportions is defined by a vector of per-ink concentrations $\mathbf{c} = \{c_p, \forall p \in \mathcal{P}\}$. Given a set of primary colors \mathcal{P} , the final absorption and scattering of the resulting mixture are given by:

$$K_{mix}(\mathbf{c}, \lambda) = \sum_{p \in \mathcal{P}} c_p K_p(\lambda), \quad (1)$$

$$S_{mix}(\mathbf{c}, \lambda) = \sum_{p \in \mathcal{P}} c_p S_p(\lambda), \quad (2)$$

where the concentrations c_p are non-negative and $\sum_{p \in \mathcal{P}} c_p \leq 1$. It is important to note here that the set of primary colors \mathcal{P} contains only the inks and not the substrate that is often approximated with ideal white [Zhao and Berns 2009]. Given the absorption and scattering of the ink mixture, we can use the Kubelka–Munk equations to predict the visible spectrum R_{mix} as:

$$R_{mix}(\mathbf{c}, \lambda) = 1 + \alpha - \sqrt{\alpha^2 + 2\alpha}, \quad (3)$$

$$\alpha = \frac{K_{mix}(\mathbf{c}, \lambda)}{S_{mix}(\mathbf{c}, \lambda)}.$$

With a known illuminant, the spectrum can be transferred to visible color using standard colorimetric equations.

4.2 Predicting Tattoo Colors

The key to applying Equation 3 lies in estimating the ink-specific absorbance and scattering. Over time, many methods have been devised to achieve this goal [Zhao and Berns 2009]. A common characteristic of these methods is that they rely on precisely depositing thin and uniform films of inks and studying their interactions. Unfortunately, due to the nature of our fabrication process, it is not feasible to apply a uniform layer of ink. Instead, the tattooing process creates tiny incisions at a high spatial frequency. As a result, we decided to adapt the material estimation procedure.

Our main observation is that the substrate effectively acts as an ink, i.e., the final color is a result of mixing the absorbance and scattering of the inks together with the substrate. In our model, we use four distinct inks (cyan, magenta, yellow, and black) applied on a substrate, all with unknown parameters. This results in ten degrees of freedom ($[4 \text{ inks} + 1 \text{ substrate}] \times [\text{absorption} + \text{scattering}]$) per spectral wavelength. To solve this system we therefore need at least ten patches of linearly independent color mixtures.

We can produce these patches by applying the inks at different concentrations. The ink concentration is a function of needle liftoff as well as ink formulation. As a result, for each liftoff at which we apply the inks, we create four more degrees of freedom, one for each colored ink. To select the liftoff at which to tattoo the inks, we conduct a preliminary experiment where we deposit black ink at varying liftoffs. From the manufactured patches, we pick 4 liftoffs that visually corresponded to 0, 25, 50, and 75 percent of ink coverage. We use the same liftoffs for each ink. Since we have a weak link between the liftoff and the estimated ink coverage, we can create linearly independent combinations by printing all ink sets where the total coverage sums up to 100 percent. This resulted in a total of 70 patches (Figure 6), even though 32 would have been mathematically sufficient. We leverage the extra patches for cross-validation of our predictive model. To estimate the spectral color of each patch, we use an X-Rite i1 3 spectrometer.



Fig. 6. The color dataset is generated by tattooing the primary inks at predefined liftoff settings in 6×6 mm squares. Notably, the line tear artifact caused by the tattoo gun failing to retract during a move command has no influence on the measurements.

Estimating the absorbance and scattering of inks is a well-known challenging problem riddled with local minima [Zhao and Berns 2009]. In order to obtain a useful predictive model we propose to apply several constraints that improve the problem formulation. First, as our model now includes the substrate we must enforce that the ink combination sums up to exactly 1 for each measured color. Additionally, we enforce that the mixing ratios decrease monotonically with increasing tattoo liftoff. Next, since real-life materials exhibit smooth spectral changes, we employ a smoothness regularizer. Fourth, during cross-validation, certain folds produced spectra belonging to unused inks such as shades of violet. We attribute this to the underconstrained nature of the problem, where several ink profiles could lead to similar color mixtures. To break this dependency, we ensure that each fold during cross-validation contains the most saturated version of each primary ink. And lastly, inspired by prior measurements of inkjet inks [Babaei et al. 2017], we limit the maximal scattering of our inks to 0.1. The above constraints lead to the following minimization problem:

$$\begin{aligned} \min_{\mathbf{c}, \mathbf{K}, \mathbf{S}} \quad & \frac{1}{|\mathcal{T}|} \sum_{t \in \mathcal{T}} \int_{\Lambda_{vis}} (R_{mix}(M_t(\mathbf{c}), \lambda) - R_t(\lambda))^2 d\lambda \\ & + \frac{w_{reg}}{|\mathcal{P}|} \sum_{p \in \mathcal{P}} \left(\|K_p''\|_{L1} + \|S_p''\|_{L1} \right), \\ \text{s.t.} \quad & \forall t \in \mathcal{T} : \sum M_t(\mathbf{c}) = 1, \\ & \forall p \in \mathcal{P}, l' > l : c_{p,l'} \leq c_{p,l} \\ & S \leq 0.1, \end{aligned} \quad (4)$$

where \mathbf{c} are the estimated concentrations of inks applied by tattooing at a fixed liftoff, \mathbf{K} and \mathbf{S} are matrices of stacked absorbance and scattering for each primary ink respectively, t is a tattooed patch from a set of patches \mathcal{T} , $|\mathcal{T}|$ is the cardinality of set \mathcal{T} , $M_t(\mathbf{c})$ selects, for each primary color, the concentration of the liftoff at which this color is used in patch t , R_{mix} is the Kubelka–Munk predictive model from Equation 3 that depends on the optimized absorbance \mathbf{K} and scattering \mathbf{S} , $R_t(\lambda)$ is measured spectra of patch t , l is the liftoff of the tattoo, and the last term is the smoothness regularizer with $w_{reg} = 0.07$. The final estimated primaries are visualized in Figure 7. The predicted absorbance and scattering have similar profiles to prior work [Babaei et al. 2017] and the estimated primary colors qualitatively match visual intuition.

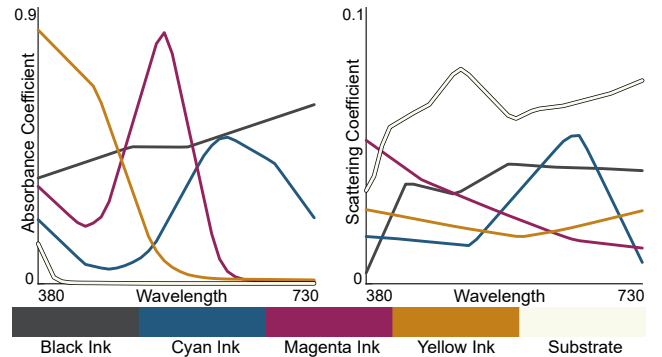


Fig. 7. Primary inks and substrate predicted by our model.

To fit the model, as well as to minimize all equations in this work, we use a constrained interior-point minimizer [Wright et al. 1999]. We validate our model using 5-fold cross-validation. To compare the measured and predicted colors, we convert the spectra into CIE L*a*b* assuming a D65 light source and a 2° standard observer. Our predictive model achieves on, average, a $2.6 \Delta E00$ color difference with a standard deviation of $1.1 \Delta E00$ and a maximal error of $5.2 \Delta E00$. Such predictions are well in line with the state-of-the-art in both 2D and 3D color printing [Babaei et al. 2017]. Figure 8 shows a subset of the colors from the testing dataset and their predictions.

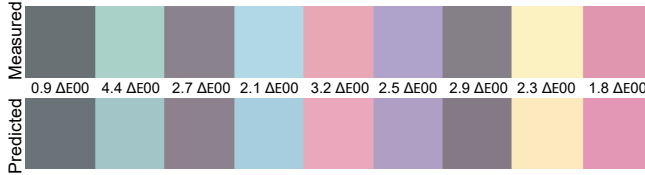


Fig. 8. Randomly selected testing data from the 5-fold cross-validation.

4.3 Color Concentration Estimation

The color prediction model associates different concentrations of primaries with visible color. To apply the model for tattooing we need to associate the concentration with machine parameters. In our setting, the color concentration is governed by the liftoff at which we apply the tattoo and the chemistry of the ink itself. We, therefore, seek a per-ink predictive model that associates the inking liftoff with color concentration. To derive this model we start by depositing color patches of individual primaries at varying liftoff. In our experiments, we start with a liftoff of 0.5 millimeters and move in 100-micron increments to 2.4 millimeters. This range was picked experimentally: below 0.5 mm the tattoo gun damaged the substrate and above 2.4 mm the color was barely visible. This results in 20 individual color samples per primary ink, Figure 9.

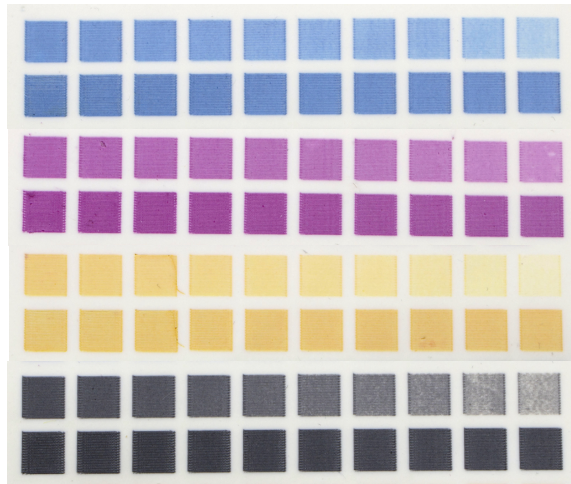


Fig. 9. Color patches generated by tattooing single colors at liftoff increasing in 100 micron increments.

Since we already know the absorbance and scattering of each ink, the only unknown to predict the color is the concentration of the ink. To find this concentration, we minimize the following equation separately for each tattooed patch:

$$\min_{c_{i,l}} \int_{\Lambda_{vis}} (R_{mix}(c_{i,l}, \lambda) - R_{i,l}(\lambda))^2 d\lambda, \quad (5)$$

where: $K_{mix} = c_{i,l}K_i + (1 - c_{i,l})K_s,$
 $S_{mix} = c_{i,l}S_i + (1 - c_{i,l})S_s,$

where $c_{i,l}$ is the optimized concentration of ink i tattooed at liftoff l , R_{mix} uses Equation 3 to predict the spectra, $R_{i,l}(\lambda)$ is the measured spectrum of ink i applied at liftoff l , and K_{mix} and S_{mix} are computed as a linear combination of the ink i and the skin substrate s based on the concentration $c_{i,l}$.

The final predicted per-ink concentrations are shown in Figure 10. We can observe that the tattoo liftoff directly correlates with the ink concentration and is well approximated by a simple linear model. A notable exception is the yellow ink, where we can observe the concentration saturates after a liftoff of 1.3 millimeters. To model this effect, we use a simple ReLU to predict the yellow concentration, i.e., we predict the concentration with the linear predictor and then apply a maximum operator. We hypothesize that, eventually, all inks would reach saturation. We observe this effect only for the yellow primary due to its overall lower concentration and our limit of minimal liftoff set to 0.5 millimeters as a conservative safety bound to avoid damaging the substrate. While this limitation could be adjusted, we did not find additional experimentation necessary as the produced color gamut was acceptable.

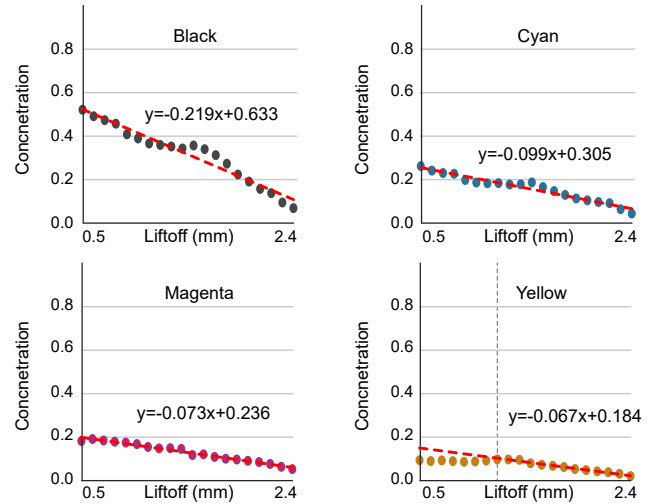


Fig. 10. Ink concentrations as a function of tattoo needle liftoff and their fit to a linear predictive model.

4.4 Color Tattoo Gamut

Finally, we investigate the color gamut of tattooing. Traditionally, color gamuts are visualized by plotting the primary inks on a chromaticity diagram. However, a trivial linear combination of the primaries is not possible in our application due to limitations of both

the possible ink concentrations (Figure 10) and combination densities (Equation 4). Therefore, to visualize the tattooing gamut, we rely on our predictive model. Since we only use a limited range of liftoffs, we can list all colors achievable by our setup and plot their convex hull on the chromaticity diagram, Figure 11. We observe that the overall lower concentrations result in a shrinking of the gamut with respect to traditional inkjet printing. However, the color gamut can nonetheless achieve a significant range of colors, especially for mixtures near the complementary set of red, green, and blue colors. Moreover, the minimum and maximum lightness achievable by our system are 30 and 97, respectively. These are notably good values, in line with commercial inkjet printers.

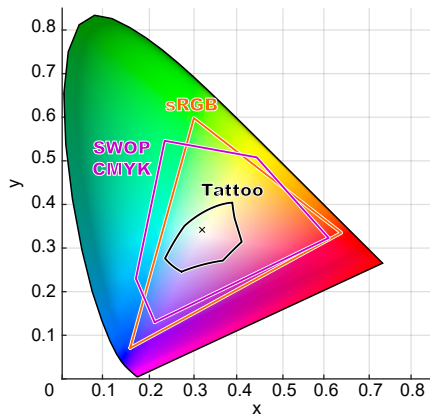


Fig. 11. Color gamut of the tattooing process (black) compared with sRGB (orange) and CMYK (violet). \times marks the substrate color.

5 SKIN COLOR SUBSTRATES

One of the aims of this work is to provide the ability to study how inks look on differently colored skin. To this end, we extend our manufacturing pipeline. To produce substrates with skin-like color, we follow standard tattoo artist training methodology by replacing a portion of the corn starch in our mixture with commercial makeup. The final mixture is composed of 1-part silicone, 0.975-part corn starch, and 0.025-part makeup.³ The final manufactured sheets can be seen in Figure 12, and were observed by the authors to faithfully represent the colors on the packaging.



Fig. 12. Color sheets fabricating by adding different makeup pigments. The names correspond to the name of the makeup shades.

The skin-like substrates contain additional pigments, therefore, to build a predictive model, we need to estimate the absorbance and

³Nyx Professional Highlight & Contour Pro Palette shades: Soft Light, Tan, Hollow, and Nyx Professional Can't Stop Won't Stop Mattifying powder - Nr. 10 Rich

scattering of each sheet. Since we are already using a known set of primary inks, we decided for a more limited experiment. We tattoo the four primary inks at the highest concentration, Figure 13. Then, we perform five spectral measurements, four of the tattooed patches and one of the substrate itself. To find the substrate parameters, we minimize a variation of Equation 4 limited to the unknown mixing concentrations and substrates absorbance and scattering:

$$\begin{aligned} \min_{c, K_s, S_s} \quad & \frac{1}{|\mathcal{T}|} \sum_{t \in \mathcal{T}} \int_{\Lambda_{vis}} (R_{mix}(M_t(c), \lambda) - R_t(\lambda))^2 d\lambda \\ & + \frac{w_{reg}}{|\mathcal{P}|} (||K_s''||_{L1} + ||S_s''||_{L1}), \\ \text{s.t. } \quad & \forall t \in \mathcal{T} : \sum M_t(c) = 1, \\ & S_s \leq 0.1, \end{aligned} \quad (6)$$

where K_s and S_s are the absorbance and scattering of the substrate, and the last term is the smoothness regularization with $w_{reg} = 0.07$.



Fig. 13. The primary inks applied on substrates with different skin colors.

The final prediction of colored substrates has an average error of $0.84 \Delta E00$ with a standard deviation of $0.64 \Delta E00$ and a maximum error of $2.22 \Delta E00$, which is well in line with our original color prediction. To further verify that the colors we manufactured correspond to realistic skin tones, we cross-referenced them with the Pantone skin tone dataset, Figure 14. We found an acceptable match for each manufactured substrate with an average $\Delta E00$ between the substrates and the Pantone colors of 2.42.



Fig. 14. The fitted color of the manufactured substrates is qualitatively similar to official skin-tones from Pantone.

5.1 Gamut of Colored Substrates

We can now investigate the gamuts of colored substrates and compare them with a plain white sheet, Figure 15. We observe that, for pale skin tones, the color gamut is practically unchanged. This is well in line with qualitative observations of tattoo artist preference for lighter skin canvases for colored tattoos. As the concentration of the pigment in the substrate increases, we note that the color gamut shrinks significantly. Moreover, the substrate white point is displaced, as darker substrates make it impossible to achieve the same neutral tone. These observations explain the challenges in providing vividly colored tattoos for clients with varying skin tones. In a later section of this paper, we will investigate how computational tools can alleviate this problem.

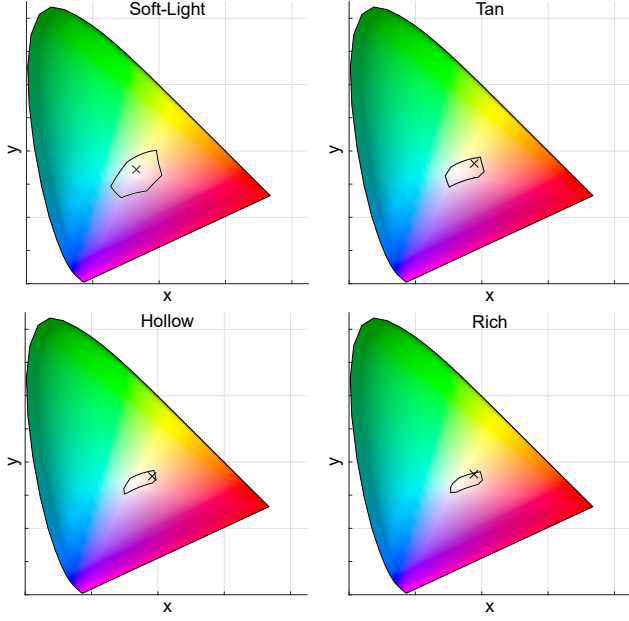


Fig. 15. Gamut of skin colored substrates get progressively smaller with darker pigments. Additionally the substrate color (marked with \times) shifts towards the gamut boundary.

6 GAMUT MAPPING FOR COLORED SUBSTRATES

Since the tattooing color gamut is limited, we need a gamut mapping strategy for fabricating colorful images. The white sheet is qualitatively similar to the regular printing substrate. Therefore, it is reasonable to assume that state-of-the-art gamut mapping methods will produce acceptable results. In our work, we opted for a modification to the method proposed by Kang et al. [2000]. For completeness, we will briefly introduce this method. The gamut mapping method works in the CIE La^*b^* color space and is composed of two steps. In the first step, we re-scale the lightness of the original image to lie within the lightness range of our tattooing device. This procedure is performed in the perceptual range of each gamut's lightness. We start by defining a sigmoidal lookup table:

$$LUT_i = \frac{1}{1 + e^{-5(i-1)/101 - 0.5}}, \quad (7)$$

where LUT_i marks the percentage to be mapped. The sigmoid is defined in such a way that the 50th percentile coincides with the mean of the target gamut lightness interval. To reconstruct the remapped lightness range, the lightness of the source gamut is first transformed through the lookup table and then re-scaled to the range of the target gamut.

Next, the method operates on hue planes. For each hue plane, two special points on the lightness axis are selected. To estimate these points for different hues, Kang et al. [2006] rely on psychophysical experiments. Since the experiments are not applicable to tattoo substrates, we use fixed focus points located at 25 and 75 percent of lightness. The colors are then divided into three groups. The colors

with lightness above and below the special point are mapped towards their corresponding point. All other colors are mapped along the chromaticity axis. This procedure is illustrated in Figure 16.

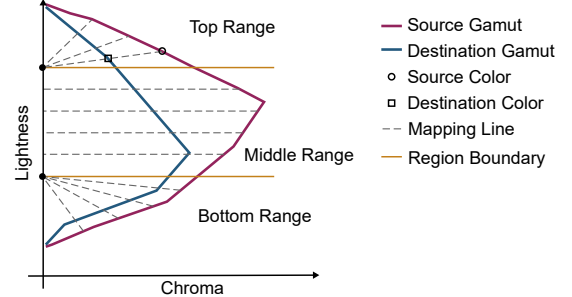


Fig. 16. To map the color from source to destination, we divide the hue plane into three regions. In the bottom and top regions, mapping is done on a line towards the corresponding extremal point. In the middle region, we map along the chromaticity axis.

While Kang's method works well for the white substrate, it does not translate well to the colored ones. The primary reason is the color shift inherent to each skin tone. We can observe this effect in Figure 17 top. As the substrate skin tone gets darker, the desired colors cannot be faithfully captured and many are clipped. We experimented with two strategies that compensate for this effect.

The first strategy is chromaticity adaptation. For each skin substrate, we used the Bradford transform [Luo and Hunt 1998] to find a mapping between the white point of the image and the white point of the substrate, Figure 17 middle. We can observe that the compensation helps to reintroduce some of the lost contrast. However, for the darkest skin tones, the chromaticity adaptation cannot maximize the available colors.

For the last strategy, we leverage our predictive model. Our model predicts the final color from a concentration. The concentration depends on the needle liftoff which is consistent across different skin substrates. Therefore, we are capable of producing a dense morphing between different skin substrates by first estimating the color on one substrate, converting the color to liftoffs using our predictive model from Figure 10, and reconstructing the color on another substrate given known liftoffs. We use this procedure to enhance the gamut mapping for colored substrates. First, we gamut map the image to a white substrate where we know state-of-the-art methods work well. Next, we morph the colors to the new substrate according to the above-described procedure. We can observe the effect of our approach in Figure 17 bottom.

Our gamut mapping strategy allowed us to regain some contrast between colors, even on the most challenging skin substrates. Moreover, it enabled a more active use of the skin substrate in the tattoo design. The price for these improvements is a significant shift in colors towards the skin white point, resulting in poorer color fidelity with respect to the original image. As the goals of a given design may vary, artistic intent can be expressed by selecting the preferred gamut mapping process for a given piece's design.

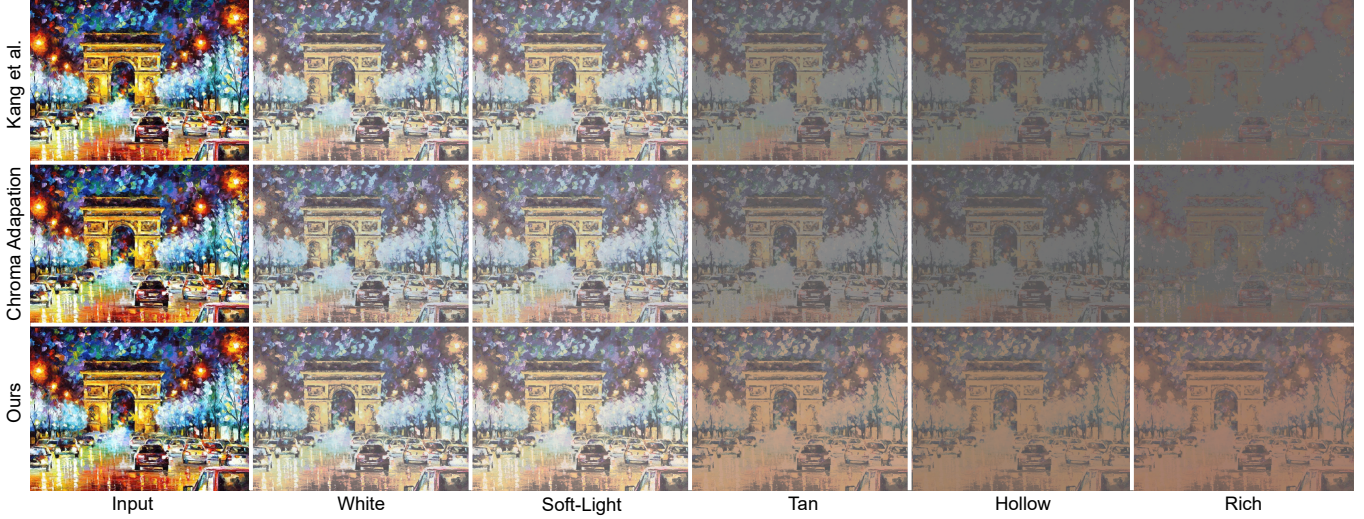


Fig. 17. Different gamut mapping strategies for optimizing color reproduction on substrates with varying skin tones. Image courtesy of © Leonid Afremov <https://afremov.com/>.

7 APPLICATIONS

In this section, we demonstrate several applications enabled by our computational tattoo machine. The ability to develop a predictive model for tattoo colors has applications towards appearance reproduction, interactive tattoo recoloring, suggesting colors for tattoo cover-ups, creating medical tattoos, enhancing tattoos with functional elements, and even optimizing for novel tattoo inks.

7.1 Color Tattoo Design

To transfer a design from image to tattoo, we start with the original image, which is then gamut mapped to a tattooing substrate. Finally, we solve the following minimization to recover the concentration of primary inks:

$$\begin{aligned} \min_{\mathbf{c}} \quad & \int_{\Lambda_{vis}} (\text{LAB}(R_{mix}(\mathbf{c}, \lambda)) - lab)^2 d\lambda, \\ \text{s.t.} \quad & \sum_{p \in \mathcal{P}} c_p = 1, \\ & \forall p \in \mathcal{P} : 0 \leq c_p \leq u_p, \end{aligned} \quad (8)$$

where \mathbf{c} are the concentrations of the primary inks, LAB transforms visible spectra to the CIE La*b* color space assuming a D65 light source and the 2° standard observer, lab is the desired color, and u_p are per-ink upper bounds on the concentration.

Once the concentrations are known, we use our linear predictive model to compute the needle liftoffs. To transfer the discrete image to a continuous tattoo machine, we employ a rasterization process. A single tattoo machine path is 209 microns thick. Therefore, we discretize each pixel as a 209 micron square. As the liftoff of each image pixel varies slightly and the tattoo machine cannot move to a new height instantaneously, we adjust the height during the first and last machine step for each pixel. The result of the tattooing process on an image is shown in Figure 18.



Fig. 18. Example color reproduction using our full pipeline. The input image (left) is gamut-mapped (middle) and then fabricated (right).

The tattooing process achieved a very high-resolution color deposition. A faint scanline rendering artifact is barely noticeable but can become apparent if the silicone skin is damaged, as was the case in the shark's jaw. However, we can note that the damage is not excessive and the original color is preserved. Another practical factor affecting color reproduction is the need to manually clean samples between different ink depositions. This cleaning process involves rubbing the surface with a solvent to remove ink from the surface of the tattoo, which can result in slight misalignment of the colors. Finally, the fabricated result has a more pronounced cyan color. From our experience, this difference corresponds to consistently tattooing at about 100 microns deeper than intended. We hypothesize that this issue is caused by limitations of our hardware setup. More specifically, the needle cartridges we used were meant for human operators, and as such a 100-micron needle-to-needle variance would be acceptable. Unfortunately, in our setup, this small difference can cause visible color shifts. A more sophisticated calibration process that accounts for the needle's maximum extended length could be employed to improve performance.

Our system has three sources of dot gain: (1) the ink is absorbed into the substrate, (2) translucency of the substrate, and (3) mechanical imprecision caused by adjusting the tattoo liftoff on-the-fly

during tattooing. We did not perform experiments to disentangle their effect. However, based on Figure 9, we can observe that tattooing single inks at constant liftoff produces crisp edges. We, therefore, believe the primary dot gain observed in Figure 18 is caused by the mechanical imprecision that is especially pronounced between regions of no-color and full-color coverage, such as the black outlines.

7.2 Interactive Tattoo Recoloring

As we have seen during our investigation of colored substrates, creating designs for darker skin tones manually is challenging. With the help of our predictive model, we can empower artists with computational tools to modify their designs. As an example, we demonstrate a possible design pipeline of a fish tattoo, given in Figure 19. Using our gamut mapping, we can see a preview of the design indicating that the yellow belly would not be visible. In order to recolor the fish, we begin by finding a lower parameter color space. A good option are color-triads that can represent the image using only three key colors [Shugrina et al. 2020]. In our example, the problematic yellow color is easily discernible. However, replacing the color manually is still not trivial. We need to ensure that the new color satisfies the following requirements: (1) the new color should be visible on the substrate, (2) the new color should maintain the relative contrast with existing colors, and (3) the new color should be harmonious with the other colors in the design. We express these requirements by formulating the following optimization:

$$\begin{aligned} \max_{\mathbf{c}} \quad & \sum_{i \in \{K, C, S\}} H(c, i) + w_{nrm} \sum_{i \in \{Y, S\}} (c, i), \\ \text{s.t. } \forall i \in \{C, M, Y, K, S\} : \Delta E00(c, i) \geq T_i, \end{aligned} \quad (9)$$

where c is the new color, K, C, Y, S is a set of the three original colors black, cyan, yellow, and the substrate, H is a binary color harmony estimator from [Ou and Luo 2006] that ensures the selected color works well with the design, $w_{nrm} = 0.054$ is a regularization weight for the last term that enforces the new color is different from the current one and contrasts with the background, and T_i is a per color threshold on minimal $\Delta E00$ to maintain contrast in the image.

For our example, the optimized output is a shade of magenta. After recomputing the tattoo and fabricating both designs, we can see that the computational tool allowed us to achieve a tattoo that maximizes the visibility of each color, (Figure 19).

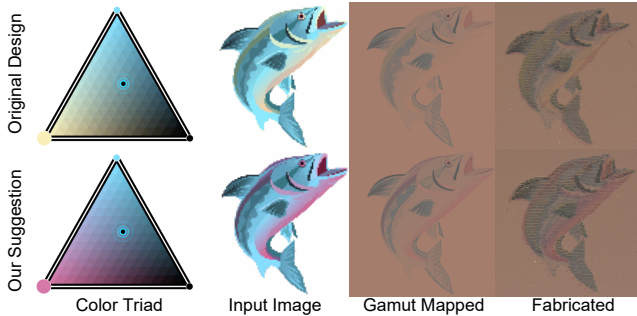


Fig. 19. The original design contains a yellow color that has low contrast with the darker substrate. We can use computation to suggest a new color that contrasts the substrate and remains harmonious with the design.

7.3 Tattoo Coverups

A common tattoo problem is to cover-up an old tattoo with a new one. This is a particularly challenging process since the new colors interact with the previously deposited inks. The non-linear nature of this interaction can produce surprising results. To avoid these issues artists typically rely on small sets of known mixtures and adjust the color by applying the difference in ink concentration between the old and new colors. However, this does not necessarily lead to optimal color reproduction. Instead, we propose to use our computational model to optimize for new colors under the constraint of the inks already applied in the skin. To this end, we solve the following optimization problem for each ink combination:

$$\begin{aligned} \min_{\mathbf{c}} \quad & \int_{\Lambda_{vis}} (\text{LAB}(R_{mix}(\mathbf{c}, \lambda)) - lab)^2 d\lambda, \\ \text{s.t. } \quad & \sum_{p \in \mathcal{P}} c_p = 1, \\ & l_p \leq c_p \leq u_p, \end{aligned} \quad (10)$$

where \mathbf{c} are the new concentrations of inks to be deposited on the surface, LAB transforms visible spectra to CIE $L^*a^*b^*$ color assuming a D65 light source and the 2° standard observer, lab is the desired color, l_p are per ink concentrations already applied in the skin, and u_p are the per-ink upper bounds on concentration.

We can see the effect of our color choice in Figure 20. In this scenario, the client would like to recolor his design from shades of green to shades of red. Applying a naive color difference leads to a noticeable green tint. In contrast, utilizing the full-color optimization allows us to get significantly closer to the intended values. The main difference is in the overall lightness of the achieved colors, which is significantly higher for the optimized variant. Quantitatively, the optimized colors are on average $3.34 \Delta E00$ closer with a maximum improvement of $5.63 \Delta E00$.

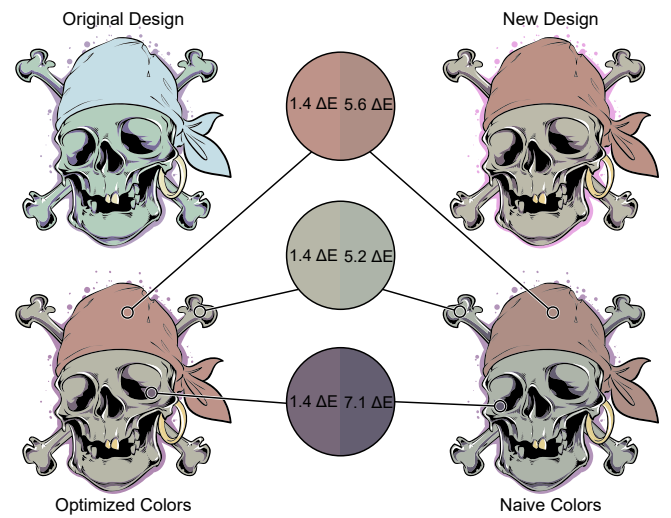


Fig. 20. Tattoo coverup by adjusting colors of an original design. By optimizing the ink mixture, we are able to achieve a significantly better match. Image courtesy of © freedesignfile.

7.4 Medical Tattoos

The ability of our system for reproducing specific colors can be useful in the medical industry to create realistic-looking prosthetics or design coverup tattoos for scar tissue. To demonstrate these capabilities, we captured a photograph of a human hand, Figure 21 left. We visually identified the soft-light artificial skin as the closest match and computed a preview of a tattoo that attempts to replicate the hand’s colors , Figure 21 middle. To quantitatively compare the images, we calculated the pixel-to-pixel ΔE^{00} error. Our reproduction pipeline achieved a mean error of 3.32 ΔE^{00} , with a standard deviation of 4.6 and a maximum error of 22 ΔE^{00} . To better visualize these discrepancies, we plot them as a grayscale map, Figure 21 right. We can observe that the major discrepancies are located in the self-shadowed areas of the original photo. This is caused by a discrepancy in our black level, which has a minimum lightness of 30. However, self-shadowing is not an intrinsic part of the hand and would appear naturally on a manufactured prosthetic. If we omit the self-shadowed regions, the color difference significantly improves to a mean error of 0.68 ΔE^{00} , with a standard deviation of 1.34 and a maximum error of 5 ΔE^{00} , we believe this demonstrates our system’s potential to reproduce skin tones of real subjects for medical applications. A possible extension of this system would involve a spectrally optimized reproduction, helping achieve good matches irrespective of the illuminant, avoiding metamerism.



Fig. 21. The color preview shows that our tattoo machine can be used to add realistic skin-features to a bulk silicone material.

7.5 Functional Tattoos

Apart from traditional ink, our tattoo prototype can also process functional materials. Of particular interest are functional inks loaded with carbon or silver particles. The ability to process such inks allows for embedding functional designs inside the tattoo medium. This embedding allows for tighter integration and the creation of abrasion-resistant circuits that are protected by the substrate. We demonstrate this capability with two exemplar designs.

The first design is an interactive touch circuit, Figure 22. We printed a conductive trace that is connected to an Arduino. Upon registering the touch, the Arduino reacts and lights up an LED. Such interactive circuits can be further expanded to create complete touch interfaces on silicone materials. For example, an animatron could be programmed to react based on where it is touched. Further, the tattooed circuit could be used to guide conductive traces on the animatron to minimize the wiring required for its operation.

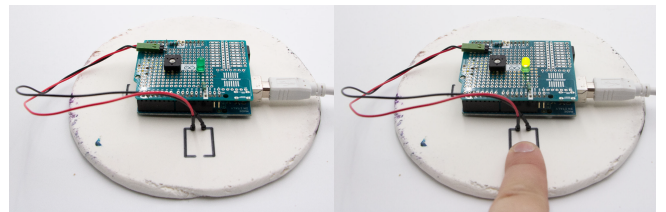


Fig. 22. Tattooed circuit acting as a touch on/off button for an LED. The circuit is embedded in the material and resistant to abrasion.

The second design is an embedded bend sensor, Figure 23. The sensor has a rest resistance of 300 k Ω . Upon deformation, the resistance changes by ± 40 k Ω , depending on the direction of the bend. Such embedded sensors have the potential to enhance prosthetics to be self-aware of their position and orientation. For example, a series of bend sensors applied on the front of the prosthetic could detect a quick bending deformation, suggesting an impact event. The prosthetic controller could then react accordingly and try to minimize the impact damage.

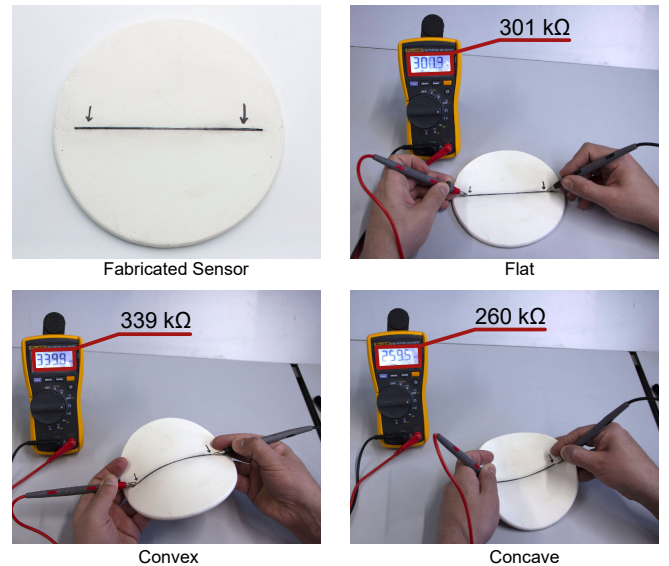


Fig. 23. A bend-sensing sensor that smoothly covers the range from convex to concave shapes.

7.6 Novel Ink Optimization

Our last example application attempts to improve the gamut of color tattoos on darker skin tone substrates. If we want to manufacture the designs in Figure 24. The target base complexion unfortunately does not allow for such bright colors. We will then use our predictive model to investigate if a different set of inks could enhance the final

colors. To this end, we solve the following optimization:

$$\begin{aligned} \min_{c_i, K_i, S_i} \quad & \int_{\Lambda_{vis}} (\text{LAB}(R_{mix}(c_i, \lambda) - lab)^2 d\lambda, \\ & + w_{reg} (||K''_i||_{L1} + ||S''_i||_{L1}), \\ \text{s.t.} \quad & c_i \leq 0.52, \\ & S_i \leq 0.1, \end{aligned} \quad (11)$$

where c_i is the concentration of the new ink. $w_{reg} = 0.07$ is the regularization weight, and K_i and S_i are the absorbance and scattering of the novel ink. To avoid the trivial solution of using a pure ink we constrain the ink concentration to the maximum ink concentration achieved in our physical samples (see Figure 10).

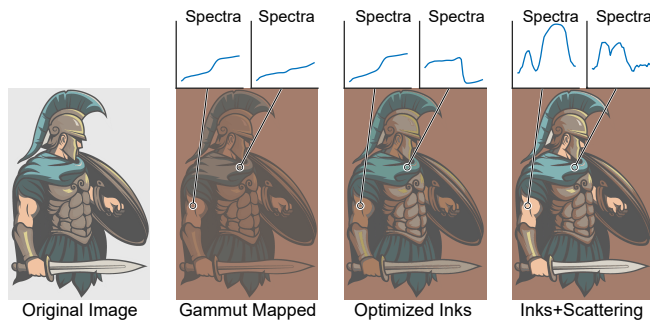


Fig. 24. Optimizing for skin-specific inks allows to produce more vivid tattoos.

We can see that a novel set of inks allowed us to push the color reproduction and achieve significantly brighter colors. We can push the boundaries even further by lifting the scattering constraints of the inks, Figure 24 right. An important next step would be the investigation of the feasibility of generating inks with these spectral profiles. Practical manufacturing constraints could be integrated with our simulation engine to produce optimal results.

8 LIMITATIONS

This paper provides the first investigation of tattooing as a fabrication process. To achieve this goal, we focused our efforts on building a practical model for tattoo appearance. However, several directions can be further explored to fully develop tattooing as a fabrication method.

In our investigation, we relied on a relatively inexpensive Cartesian robot coupled with an inexpensive tattoo gun. While such a system enables initial exploration, it is also limited by hardware constraints. In particular, the tattoo needles have a relatively small needle-to-needle variance, which has a visible influence on the final color in our setting. Moreover, the gantry provides only 10-micron steps and has unknown repeatability. To achieve high-quality spectral reproduction, finer steps and low repeatability errors are essential.

The substrates we employ are a mixture of silicone, cornstarch, and a pigment. While adequate for initial exploration, there is still a domain gap between the complex behavior of human skin and our artificial sheets. A clear improvement would lie in adjusting the

pigment mixing in our sheets to be able to generate skin-like substrates with desired spectral colors. Another potential improvement is replacing cornstarch with a translucent ink-absorbent medium, to enable control over both color and translucency.

As our primary inks, we selected off-the-shelf inkjet colors based on ease of access. While these are not used for tattoos on humans in practice, we employ them as a proof of concept demonstrating a quantified model of tattoos on artificial skin. An interesting direction for future work would be to model and include more tattoo inks. Such a system would then benefit from novel ink-selection algorithms [Ansari et al. 2020] to further improve the spectral match of the tattooed colors.

Applying our color prediction model to human skin requires measuring its optical properties and understanding how it absorbs ink. The main challenge lies in estimating the true appearance of heterogeneous skin, even in non-flat regions with potentially glossy finishes from skin oils. We believe this is an exciting avenue for future work. A promising direction is to leverage our model to reverse-engineer existing tattoos: Given a spectral capture of a tattoo and ink parameters, our model could be used to estimate the spatially-varying skin properties and ink absorbance.

Finally, we provide a glimpse into many applications of our tattoo system, such as color reproduction, skin-tone specific gamut mapping, interactive tools for tattoo recoloring, full skin replication, functional tattoos, and personalized ink optimization. While exciting in their own right, each of these applications merit further study.

9 CONCLUSION

We present the first systematic study of tattooing as a computational fabrication process. To this end, we constructed a numerically controlled tattoo machine and provided a repeatable recipe for artificial skin manufacturing. We built a predictive model that can estimate the perceived tattoo appearance based on the parameters of the tattoo machine. We investigate both plain white substrates, as well as substrates aiming to simulate a variety of skin tones. While our skin tone estimation is performed on artificial silicone sheets, the insights gained towards color mapping on various substrates should hold as general guidelines even for real skin. We hope that the tools presented in this work will enable a more inclusive environment, where tattoo artists employing computational tools are able to deliver colorful tattoos that match client expectations regardless of skin tone. Moreover, we demonstrate that tattooing as a fabrication process can go beyond appearance and integrate functional circuits and printed sensors into the tattoo design. We hope that this work is the first step in leveraging this powerful color application technique by artists, makers, and researchers.

ACKNOWLEDGMENTS

We thank Todor Asenov and the Miba Machine Shop for their help in assembling the tattoo machine and manufacturing the substrates. We thank Geysler Rodrigues for the insightful discussions on tattooing practices from a professional artist's perspective. We thank Maria Fernanda Portugal for sharing a doctor's perspective on medical applications of tattoos. The artwork for Figure 17 was provided

by Leonid Afremov. His original work is available at afremov.com. The artwork for Figure 20 was provided by freedesignfile under the Creative Commons license. The original is available at all-free-download.com. This work is graciously supported by the FWF Lise Meitner (Grant M 3319).

REFERENCES

- Matthew Anderson, Ricardo Motta, Srinivasan Chandrasekar, and Michael Stokes. 1996. Proposal for a standard default color space for the internet—srgb. In *Color and imaging conference*, Vol. 1996. Society for Imaging Science and Technology, 238–245.
- Navid Ansari, Omid Alizadeh-Mousavi, Hans-Peter Seidel, and Vahid Babaei. 2020. Mixed Integer Ink Selection for Spectral Reproduction. *ACM Trans. Graph.* 39, 6, Article 255 (nov 2020), 16 pages. <https://doi.org/10.1145/3414685.3417761>
- Vahid Babaei, Kiril Vidimće, Michael Foshey, Alexandre Kaspar, Piotr Didyk, and Wojciech Matusik. 2017. Color Contoning for 3D Printing. *ACM Trans. Graph.* 36, 4, Article 124 (jul 2017), 15 pages. <https://doi.org/10.1145/3072959.3073605>
- Roy S Berns. 2019. *Billmeyer and Saltzman's principles of color technology*. John Wiley & Sons.
- Alan Brunton, Can Ates Arıkan, and Philipp Urban. 2015. Pushing the limits of 3D color printing: error diffusion with translucent materials. *ACM Transactions on Graphics (TOG)* 35, 1 (2015), 1–13.
- Danwu Chen and Philipp Urban. 2021. Deep learning models for optically characterizing 3D printers. *Optics Express* 29, 2 (2021), 615–631.
- Craig Donner, Tim Weyrich, Eugen d’Eon, Ravi Ramamoorthi, and Szymon Rusinkiewicz. 2008. A layered, heterogeneous reflectance model for acquiring and rendering human skin. *ACM transactions on graphics (TOG)* 27, 5 (2008), 1–12.
- Oskar Elek, Denis Sumin, Ran Zhang, Tim Weyrich, Bernd Bickel, and WILKIE ALEXANDER. 2017. Sca ering-aware Texture Reproduction for 3D Printing. (2017).
- Louise Finlayson, Isla RM Barnard, Lewis McMillan, Sally H Ibbotson, C Tom A Brown, Ewan Eadie, and Kenneth Wood. 2022. Depth penetration of light into skin as a function of wavelength from 200 to 1000 nm. *Photochemistry and Photobiology* 98, 4 (2022), 974–981.
- Geeta Garg and Gurvinder P Thami. 2005. Micropigmentation: tattooing for medical purposes. *Dermatologic surgery* 31, 8 (2005), 928–931.
- Chet S Haase and Gary W Meyer. 1992. Modeling pigmented materials for realistic image synthesis. *ACM Transactions on Graphics (TOG)* 11, 4 (1992), 305–335.
- Garrett M Johnson and Mark D Fairchild. 2003. A top down description of S-CIELAB and CIEDE2000. *Color Research & Application: Endorsed by Inter-Society Color Council, The Colour Group (Great Britain), Canadian Society for Color, Color Science Association of Japan, Dutch Society for the Study of Color, The Swedish Colour Centre Foundation, Colour Society of Australia, Centre Français de la Couleur* 28, 6 (2003), 425–435.
- BH Kang. 2000. Gamut compression algorithm development using observer experimental data. *Proc. Colour Imaging Science 2000* (2000).
- Byoung-Ho Kang, Min-Ki Cho, Heui-Keun Choh, and Chang-Yeong Kim. 2006. Perceptual gamut mapping on the basis of image quality and preference factors. In *Color Imaging XI: Processing, Hardcopy, and Applications*, Vol. 6058. SPIE, 52–60.
- Paul Kubelka. 1931. Ein Beitrag zur Optik der Farbanstriche (Contribution to the optic of paint). *Zeitschrift für technische Physik* 12 (1931), 593–601.
- Tom Lister, Philip A Wright, and Paul H Chappell. 2012. Optical properties of human skin. *Journal of biomedical optics* 17, 9 (2012), 090901–090901.
- MR Luo and RWG Hunt. 1998. The structure of the CIE 1997 colour appearance model (CIECAM97s). *Color Research & Application: Endorsed by Inter-Society Color Council, The Colour Group (Great Britain), Canadian Society for Color, Color Science Association of Japan, Dutch Society for the Study of Color, The Swedish Colour Centre Foundation, Colour Society of Australia, Centre Français de la Couleur* 23, 3 (1998), 138–146.
- Office for Science and Society McGill University. 2017. *What is The History of Tattoos?* <https://www.mcgill.ca/oss/article/history-you-asked/what-history-tattoos>
- Charles Mignon, Desmond J Tobin, M Zeitouny, and NE Uzumbajakava. 2018. Shedding light on the variability of optical skin properties: finding a path towards more accurate prediction of light propagation in human cutaneous compartments. *Biomedical optics express* 9, 2 (2018), 852–872.
- Ján Morovič. 2008. *Color gamut mapping*. John Wiley & Sons.
- Garrett Munice. 2021. *Everything You Need to Know About Tattooing on Darker Skin*. <https://www.menshealth.com/grooming/a35658654/tattoos-on-dark-skin/>
- Hans EJ Neugebauer. 1937. Die theoretischen grundlagen des mehrfarbenbuchdrucks. *Zeitschrift für Wissenschaftliche Photographie. Photophysik und Photochemie* 36, 4 (1937), 73–89.
- Thomas Klaus Nindel, Tomáš Iser, Tobias Rittig, Alexander Wilkie, and Jaroslav Krivánek. 2021. A gradient-based framework for 3D print appearance optimization. *ACM Transactions on Graphics (TOG)* 40, 4 (2021), 1–15.
- Li-Chen Ou and M. Ronnier Luo. 2006. A colour harmony model for two-colour combinations. *Color Research & Application* 31, 3 (2006), 191–204. <https://doi.org/10.1002/cola.20208> arXiv:<https://onlinelibrary.wiley.com/doi/pdf/10.1002/col.20208>
- Marios Papas, Christian Regg, Wojciech Jarosz, Bernd Bickel, Philip Jackson, Wojciech Matusik, Steve Marschner, and Markus Gross. 2013. Fabricating translucent materials using continuous pigment mixtures. *ACM Transactions on Graphics (TOG)* 32, 4 (2013), 1–12.
- Michał Piorvarci, Michael Foshey, Vahid Babaei, Szymon Rusinkiewicz, Wojciech Matusik, and Piotr Didyk. 2020. Towards spatially varying gloss reproduction for 3D printing. *ACM transactions on graphics* 39, 6 (2020).
- Dana Pokorna, Ivonne Rubio, and Martin Müller. 2008. DNA-vaccination via tattooing induces stronger humoral and cellular immune responses than intramuscular delivery supported by molecular adjuvants. *Genetic Vaccines and therapy* 6, 1 (2008), 1–8.
- Clinton Sanders and D Angus Vail. 2008. *Customizing the body: The art and culture of tattooing*. Temple University Press.
- Liang Shi, Vahid Babaei, Changil Kim, Michael Foshey, Yuanming Hu, Pitchaya Sithithumrong, Szymon Rusinkiewicz, and Wojciech Matusik. 2018. Deep multispectral painting reproduction via multi-layer, custom-ink printing. *ACM Transactions on Graphics* (2018).
- Maria Shugrina, Amlan Kar, Sanja Fidler, and Karan Singh. 2020. Nonlinear Color Triads for Approximation, Learning and Direct Manipulation of Color Distributions. *ACM Trans. Graph.* 39, 4, Article 97 (aug 2020), 13 pages. <https://doi.org/10.1145/3386569.3392461>
- Sárka Sochorová and Ondřej Jamríška. 2021. Practical pigment mixing for digital painting. *ACM Transactions on Graphics (TOG)* 40, 6 (2021), 1–11.
- Maureen C Stone, William B Cowan, and John C Beatty. 1988. Color gamut mapping and the printing of digital color images. *ACM Transactions on Graphics (TOG)* 7, 4 (1988), 249–292.
- Denis Sumin, Tobias Rittig, Vahid Babaei, Thomas Nindel, Alexander Wilkie, Piotr Didyk, Bernd Bickel, J Krivánek, Karol Myszkowski, and Tim Weyrich. 2019. Geometry-aware scattering compensation for 3D printing. *ACM Transactions on Graphics* 38, 4 (2019).
- Philipp Urban, Tejas Madan Tanksale, Alan Brunton, Bui Minh Vu, and Shigeki Nakuchi. 2019. Redefining a in rgba: Towards a standard for graphical 3d printing. *ACM Transactions on Graphics (TOG)* 38, 3 (2019), 1–14.
- Snejina Vassileva and Evgeniya Hristakieva. 2007. Medical applications of tattooing. *Clinics in dermatology* 25, 4 (2007), 367–374.
- Ian L Weatherall and Bernard D Coombs. 1992. Skin color measurements in terms of CIELAB color space values. *Journal of investigative dermatology* 99, 4 (1992), 468–473.
- James Withee. 2018. *Tattoo Advice for People with Dark Skin*. <https://www.youtube.com/watch?v=Xlj0hfV0Nba>
- Stephen Wright, Jorge Nocedal, et al. 1999. Numerical optimization. *Springer Science* 35, 67–68 (1999), 7.
- Gunter Wyszecki and Walter Stanley Stiles. 1982. *Color science*. Vol. 8. Wiley New York.
- X-Rite. 2005. Complete Guide to Color Management. https://xritephoto.com/documents/literature/en/L11-176_Guide_to_CM_en.pdf. (2005). Accessed: 2023-01-22.
- JAC Yule and WJ Nielsen. 1951. The penetration of light into paper and its effect on halftone reproduction. In *Proc. TAGA*, Vol. 3. 65–76.
- Yonghui Zhao and Roy S. Berns. 2009. Predicting the spectral reflectance factor of translucent paints using Kubelka-Munk turbid media theory: Review and evaluation. *Color Research & Application* 34, 6 (2009), 417–431. <https://doi.org/10.1002/col.20525> arXiv:<https://onlinelibrary.wiley.com/doi/pdf/10.1002/col.20525>
- Arthur Zuckerman. 2020. *38 Tattoo Statistics: 2020/2021 Industry, Trends & Demographics*. <https://comparecamp.com/tattoo-statistics/>